Journal of Energy Storage 50 (2022) 104221

Contents lists available at ScienceDirect

Journal of Energy Storage

journal homepage: www.elsevier.com/locate/est

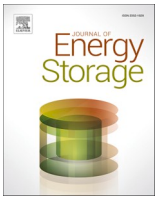

Research Papers

Integration of fully printed and flexible organic electrolyte-based dual cell supercapacitor with energy supply platform for low power electronics

Chakra Rokaya *, Jari Keskinen, Donald Lupo

Faculty of Information Technology and Communication Sciences, Tampere University, Korkeakoulunkatu 3, Tampere FI-33720, Finland

ARTICLE INFO

Keywords:
Dual cell supercapacitor
Electrolyte
Ambient
Harvester
Power
Organic photovoltaic cell
Energy supply platform
Energy storage

ABSTRACT

We report the fabrication of flexible, printed dual cell supercapacitors (DCSCs) and their implementations in energy storage units providing peak power to portable devices. The use of organic electrolytes enhances higher capacity in both potential windows (2.5 V/cell) and the temperature ranges than the aqueous electrolytes, while propylene carbonate retains the advantages of low cost and low toxicity. The device delivered capacitance value between 3 and 4 mF, equivalent series resistance $< 2\ \Omega$, and very low leakage current of about 0.1 μA. We demonstrated the integration of an organic photovoltaic module (OPV) with an energy supply platform (ESP) and DCSCs for indoor light energy harvesting and storage. The maximum harvested energy was about 39 mJ. The energy is sufficient to provide peak power to portable devices and sensors. This was confirmed by powering an LED with our energy harvesting system. Mechanical deformation testing of DCSCs shows excellent mechanical stability, so that the device is well suited for flexible energy storage units. In a long-term cyclic stability test, the decrease in capacitance value was only 1% of the initial value after 10,000 cycles, indicating good durability and performance.

1. Introduction

Research on energy storage devices is a need in today's world to handle environmental and energy issues, which have attracted growing interest in the last decades. Energy storage devices store harvested energy and act as a backup source to provide energy when the primary energy source is not available [1,2]. The main energy storage devices are batteries and supercapacitors. Supercapacitors are a promising and emerging technology [3] for environmentally friendly and low-cost energy harvesting and storage systems in which a traditional battery technology is frequently not the best system, due to toxic or corrosive components, limited peak discharge current, and limited cycle life [4].

Supercapacitors, also known as electric double-layer capacitors (EDLC) [4] or ultracapacitors, have higher power densities than batteries, high efficiency, long cycle life, wide temperature ranges [3,5], quick charging time, high compatibility and no risk of explosion [6]. Supercapacitors are used to provide short term peak power in energy applications such as sensors, active RFID tags, radio transmission, Internet of Things (IoT) [7] and can operate in a wide range of temperature from about -40 °C to 100 °C [2,8,9]. In general, a supercapacitor assembly consists of current collectors, electrodes, electrolyte, and separator. Supercapacitors operate at low voltage due to the limited electrochemical window of the electrolyte. With aqueous electrolytes, the maximum potential between electrodes is about 1.3 V, whereas organic electrolytes give a maximum potential of about 3.3 V, thus can provide wider potential window and temperature range than an aqueous electrolyte [2,10].

Energy harvesting from renewable and sustainable sources has became popular in the past decade due to advances in ultralow-power electronics [11]. Flexible energy storage systems are needed for a variety of wearable, low weight, and portable electronics. Ambient energy sources such as heat, light, sound, wind, and vibration can be converted into electrical energy. The practice is called energy harvesting [12]. Previously, we have reported the use of piezoelectric energy harvesters to operate low-power devices [13].

In this paper, we focus on fully printed dual cell supercapacitors (abbreviation: DCSCs) and indoor-light energy harvesting systems which have three main parts: organic photovoltaic (Infinity OPV), energy supply platform (ESP, Epeas) and a supercapacitor (DCSC) as a storage unit. Among different energy sources, light is the most abundant source of the energy and available from indoor light sources such as a fluorescent tube, halogen lamp or LED, as well as outdoors or in indoor

* Corresponding author.
E-mail address: chakra.rokaya@tuni.fi (C. Rokaya).

https://doi.org/10.1016/j.est.2022.104221
Received 12 November 2021; Received in revised form 31 January 2022; Accepted 11 February 2022

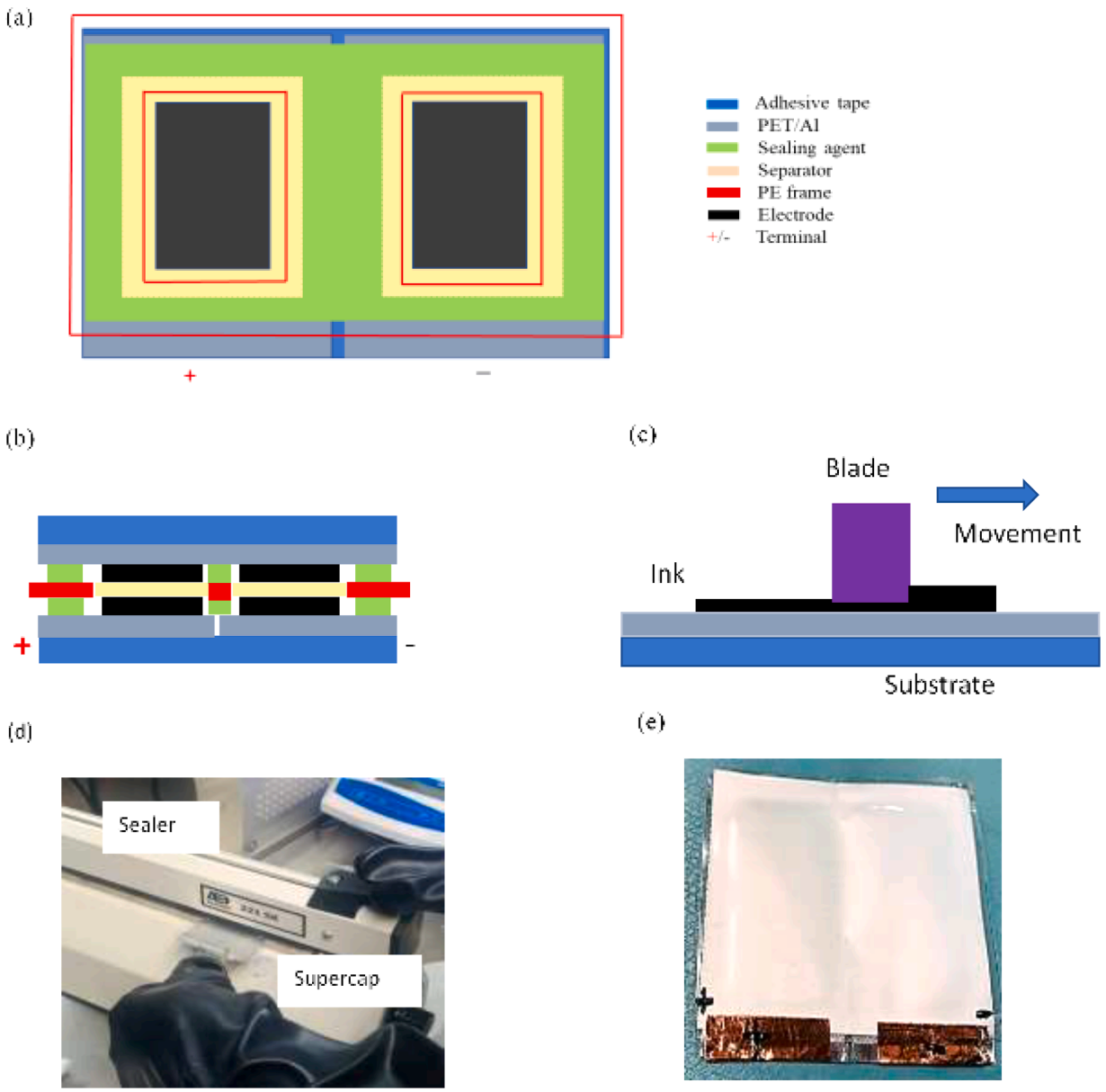

Fig. 1. Schematic drawing of dual cell series connected supercapacitor (a, b), Doctor blade coating method (c), Photograph of supercapacitor assembling inside glovebox (d), Fabricated supercapacitor (e). The layer thickness is not to scale.

spaces with windows directly from the sun [14]. Progress in efficient solar cell technology has attracted interest from researchers as well as developers and producers, and quite good low cost solar modules, including flexible modules based on polymers (OPV) are commercially available [15]. Recently, the fabrication of flexible, lightweight, wearable self-powered solar capacitors has been reported. The systems consist of flexible energy harvesting and energy storage module. The system exhibits excellent robustness and mechanical stability for many wearable scenarios. The power conversion efficiency reported was between 10.8 and 14.14% [16,17]. OPV output current is proportional to its active area and can be scaled depending on output energy requirement. Generally, the energy obtainable from ambient indoor light using commercial OPVs is in the range between 10 and 100 μW/cm^2 [18,19]. The modules used in this study, from Infinity PV, have a high degree of flexibility, low weight, thin (<0.5 mm) structure, and are easy to integrate with ESP and supercapacitor. The OPV was characterized with a standard cell testing method, AM1.5 spectrum (1000 W/m^2, one sun illumination). The OPV module used in this work is rated to have a power conversion efficiency of 5 %, which would deliver an output power of 50 W/m^2 at AM1.5. In far weaker indoor light (approximately 1/100 of AM1.5), the output power is about 0.5 W/m^2[20].

Earlier publications describe conventional direct integration of OPV with supercapacitor without a power management IC as a simple stacked device to harvest and store energy. For extremely low-cost systems, this may be adequate, but such an approach has several disadvantages such as low energy conversion, charge imbalance, inefficiency, large power dissipation etc. [21,22]. To mitigate these problems, we used an energy supply platform (ESP): (an E-peas AEM10941 conversion and control full-featured power management circuit board) that acts as an interface between OPV and supercapacitor module. The ESP consists of an ultra-low-power DC-DC buck-boost converter which operates with input voltage in the range from 0.5 V to 5 V and boosts the OPV input voltage to the adjustable output voltage range 2.2–4.5 V. The ESP system provides multiple advantages, such as OPV optimal voltage conditions at maximum power point (MPP) up to 90 %, balance of charge across the dual cell supercapacitor, device protection, increased efficiency of collecting energy, load balance standardization, and regulated power to load by high-efficient low drop output (LDO) regulators [22,23]. The

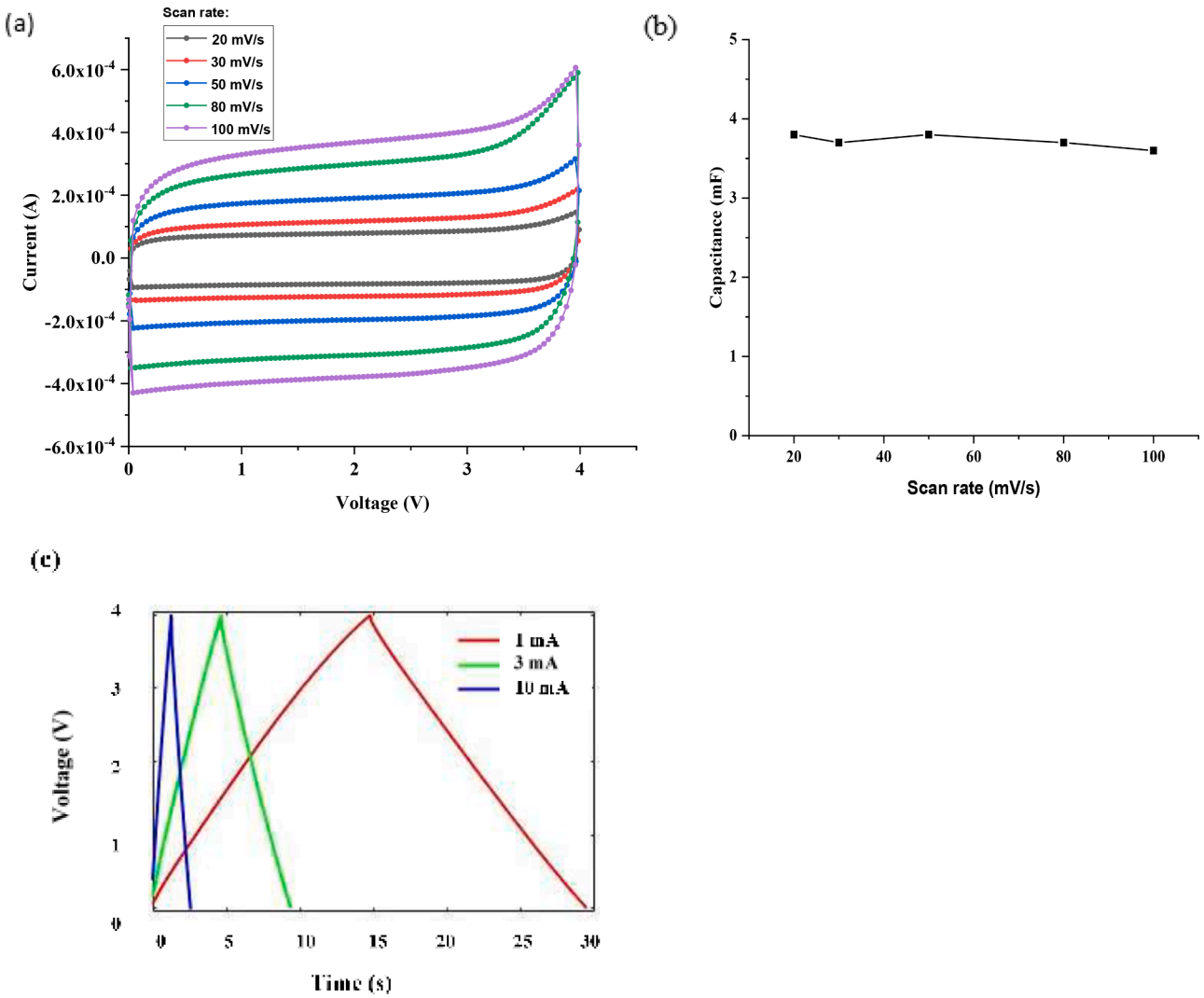

Fig. 2. Cyclic voltammetry measurement (a), Capacitance vs scan rate (b), Charge-discharge measurement (c).

targeted application requires designing of the supercapacitor properties based on the needs of the system. The choices of materials such as electrode ink, electrolyte, and current collector affect the electrical behavior of the supercapacitor in terms of voltage, capacitance, equivalent series resistance (ESR), and device flexibility. In addition to the need for higher voltage per cell and low ESR, scaling and design of the supercapacitor was important. We have previously reported printed supercapacitors for energy storage devices in the range of 100–500 mF [14,24–26]. Activated carbon ink was used to achieve high capacitance because of its high specific surface area, about 1500–2000 m^2/g. In this paper, we mainly focus on dual cell (2.5 V/cell) supercapacitors in the range of 3,4 mF to store a small amount of energy that provides sufficient peak power for low energy circuitry or radio transmission. The cells are prepared by depositing pairs of electrodes onto substrates and laminating them into devices which are connected in series internally to provide a maximum potential of 5 V. Super P conductive carbon ink was used to achieve low capacitance because of its relatively low specific surface area of about 62 m^2/g and good conductivity that would give improved ESR. Propylene carbonate (PC) electrolyte was used to achieve the targeted voltage range. PC electrolytes have good electrochemical performance, wide temperature range and low toxicity and are thermally stable, safe and relatively inexpensive. Costs are calculated based on the energy consumption and materials costs for the developed device. A cost analysis of the energy storage devices such as supercapacitors, batteries has been reported previously [27]. Like the previously reported aqueous printed supercapacitors, these are also environmentally friendly, and can be fabricated by low-cost printing processes at low temperature (<100 °C), although the final assembly requires a water-free atmosphere. Bending tests on the supercapacitor demonstrate good mechanical stability, while cyclic charge-discharge test demonstrates high cycling stability. Thus, these devices are well suited for flexible energy storage in harvesting and storage systems for distributed electronics.

2. Experimental

The schematic structure of the flexible dual cell supercapacitor is shown in Fig. 1(a & b). The fabrication process for this type of printed supercapacitors has been reported earlier [4,24,25,28,29] and is also summarized here. A polyethylene terephthalate and aluminum (PET/Al, Pyroll, thicknesses 50 μm and 9 μm, respectively) substrate size 6 cm by 5 cm was used as a current collector. The electrode material consisted of a mixture of highly conductive Super P carbon (Timcal) and carboxymethyl cellulose (CMC) binder, amounts 90 wt% and 10 wt%, respectively and deionized water to suitable viscosity. The electrodes were printed on the current collector (substrate) with laboratory-scale doctor blade coating method (Mtv Messtechnik) shown in Fig. 1(c). The wet thickness of the ink layer was about 100 μm and the area was 2 cm by 3 cm. The electrodes were cured at 60 °C for 15 min. All prints were weighed before and after applying the carbon ink in order to

Table 1
Measurement of electrical parameters of DCSCs.

S/N	Capacitance (mF)	Capacitance(F/g)	Leakage current (μA)	ESR (Ω)
DCSC1	3.0	0.130	0.10	1.8
DCSC2	3.6	0.125	0.25	2.3
DCSC3	3.9	0.110	0.30	2.4
DCSC4	4.0	0.116	0.24	2.5

determine the specific capacitance from the electrode mass. Once the electrodes were prepared, Paramelt Aquaseal X2277 adhesive was applied on the edges of PET/Al and cured at 80 °C for 20 min.

Once the adhesive was cured, electrodes were immediately transferred to a nitrogen-filled glove box for electrolyte filling and assembly under very clean and dry conditions (O_2 and H_2O concentration lower than 3 ppm). Then, 1 M tetraethylammonium tetrafluoroborate ($TEABF_4$) in propylene carbonate (PC) electrolyte was prepared inside the glove box. A polyethylene (PE) frame was added between the electrodes to prevent a short circuit. The supercapacitors were then assembled by sandwiching bottom electrodes, separators (Dreamweaver) size 3.5 cm by 2.5 cm and top electrodes as shown in Fig. 1(d). The separator and electrodes were soaked with electrolyte before assembling to ensure complete filling of the pores. Finally, the system was heat sealed in a face to face configuration with an impulse heat sealer. At the end, 50 μm thick copper tape (3M) was attached to current collectors for robust electrical contact, as shown in Fig. 1(e). The total thickness of the supercapacitor with the packaging was about 0.5 mm, with the length and breadth being 6 cm and 5 cm, respectively.

A Zennium electrochemical workstation (Zahner Elektrik GmbH) was used for cyclic voltammetry (CV) measurements of the supercapacitor. In this method, the supercapacitor was connected to the Zahner workstation. The Zennium CV software allows adjusting the lower and upper potential, number of sweeps, sampling rate etc.

3. Results and discussion

3.1. Cyclic voltammetry (CV) measurement

Cyclic voltammetry is a common method in electrochemical studies and is typically performed using a potentiostat. The value of capacitance was calculated using the formulas given in Eqs. (1) & (2) [30,31]. CV sweeps were measured at different scan rates from 20 mV/s to 100 mV/s at voltage range from 0 to 4 V as shown in Fig. 2(a). The measured

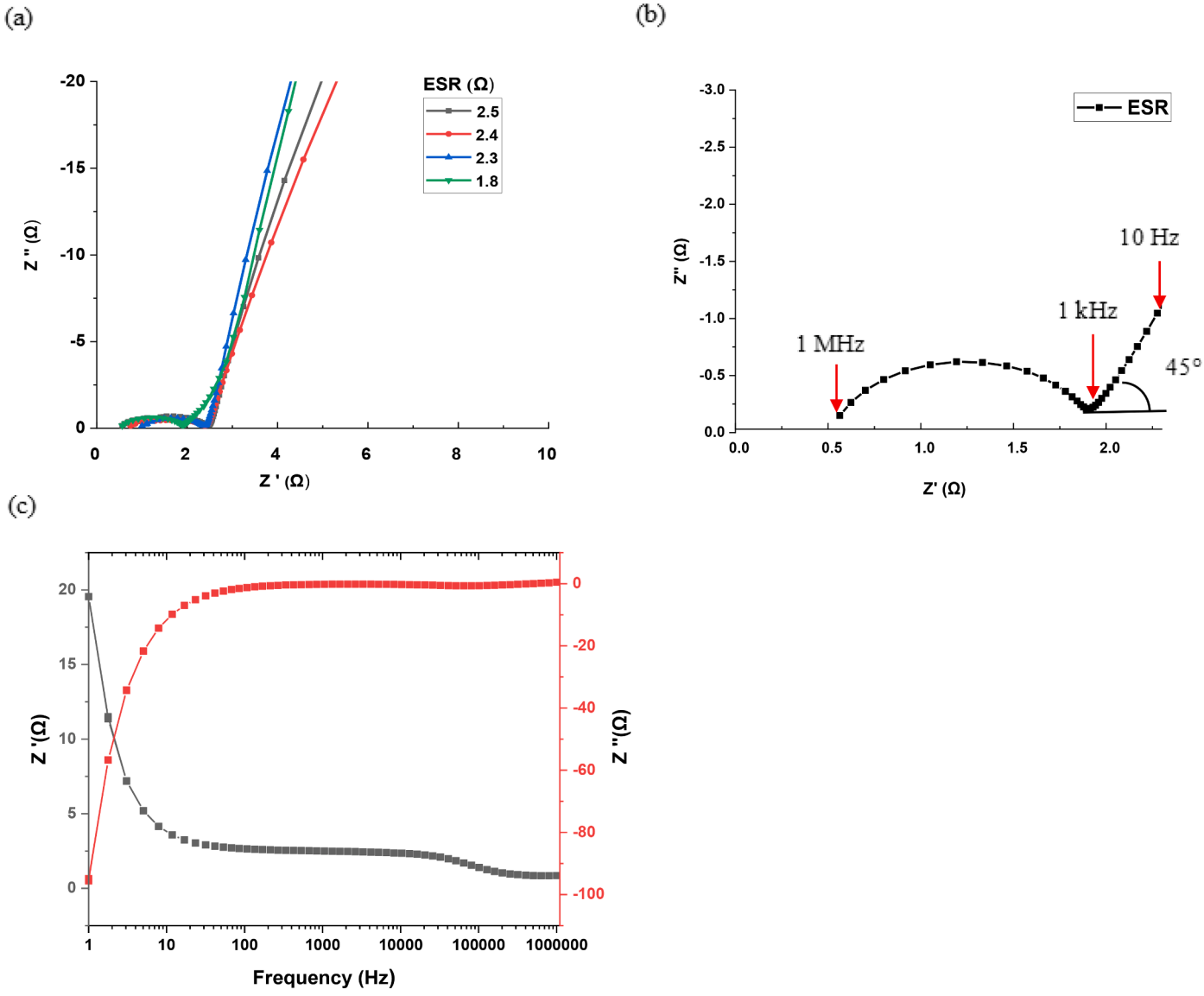

Fig. 3. Nyquist plot real and imaginary impedance (a), Magnified view of Nyquist plot (b), Plot of real and imaginary impedance as a function of frequency (c).

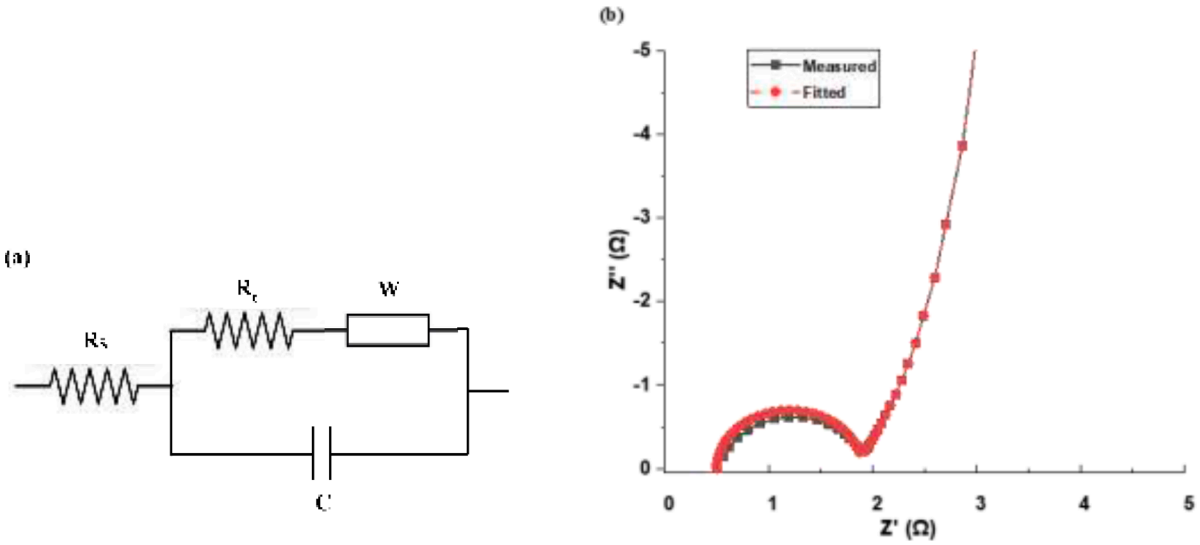

Fig. 4. Randles equivalent circuit model (a), Nyquist plot real and imaginary impedance (Measured and fitted)(b).

capacitance at a different scan rate of device DCSC1 is from 3.6 to 3.9 mF as shown in Fig. 2(b). In total four devices (DCSC1 to DCSC4) were measured for comparison (Table 1).

If V(t) is an applied voltage to the supercapacitor, the current is defined by Eq. (1).

$$I(t) = C\frac{dV}{dt} \tag{1}$$

The capacitance value is defined by Eq. (2).

$$C = \frac{I(t)}{dV/dt} \tag{2}$$

where dV/dt is the scan rate.

The capacitance value for these DCSCs is in the range between 3 and 4 mF, as expected due to the low specific area of the electrode ink. CV curves of the capacitors exhibit approximately symmetric rectangular shapes, implying relatively ideal capacitive behaviors of the cells. The galvanostatic charge-discharge curve of the DCSC at a constant current of 1 mA, 3 mA and 10 mA is shown in Fig. 2(c). The applied potential range is from 0 to 4 V. The charging curves of the DCSC are symmetrical with their corresponding discharging curves. This indicates excellent capacitive characteristics as well as the performance of the DCSC. In addition, almost linear voltage-time curves indicate that the Super P carbon ink has good electrode stability [31,32].

3.2. Electrochemical impedance spectroscopy

Electrochemical impedance spectroscopy (EIS) is an electrochemical technique frequently used for the characterization of supercapacitors to obtain information such as capacitance, conductivity, components contributing to the equivalent series resistance, real and imaginary impedances with Nyquist plot and phase angle behavior as a function of frequency with Bode plot method. The importance of EIS has been reported earlier in general, and also for EDLCs [8,29,30,33–39].

In EIS, an AC potential is applied to an electrochemical cell and the amount of current flowing through the cell is measured. The potential excitation is a sinusoidal signal and the response to this is an AC current signal. This AC current signal in the cell contains the excitation frequency and its harmonics. In our EIS measurement, the excitation frequency was in the range from 1 Hz to 1 MHz, with a small excitation signal amplitude of 10 mV. The resulting impedance Z is a complex number. The Nyquist plot of four DCSCs is shown in Fig. 3(a).

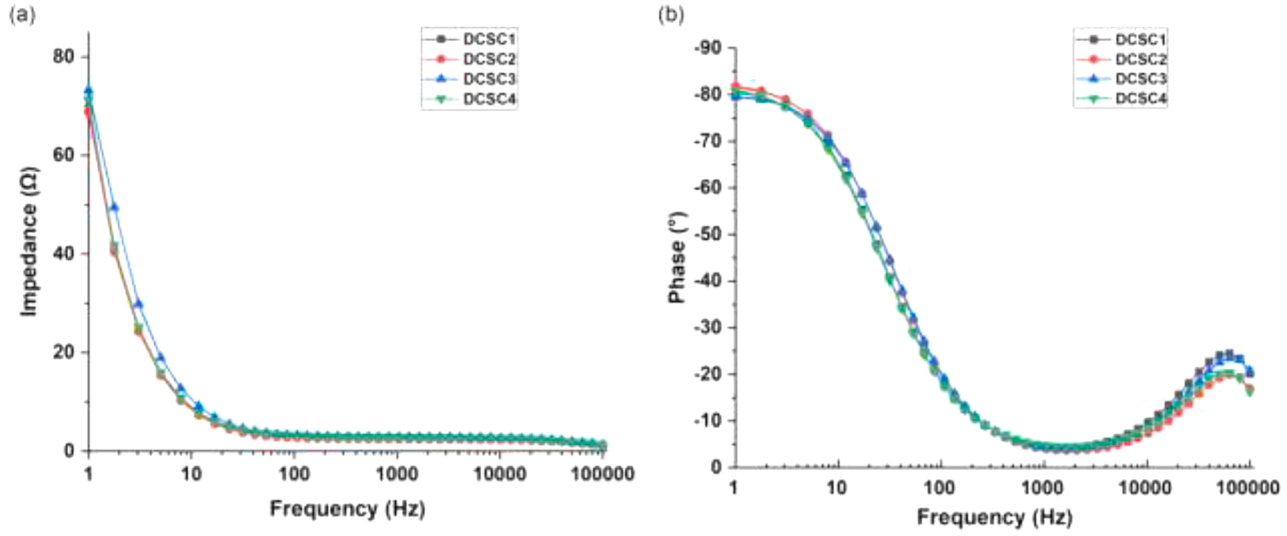

Fig. 5. Bode plot analysis of dual cell supercapacitors. Plot of impedance vs frequency (a), Plot of phase angle vs frequency (b).

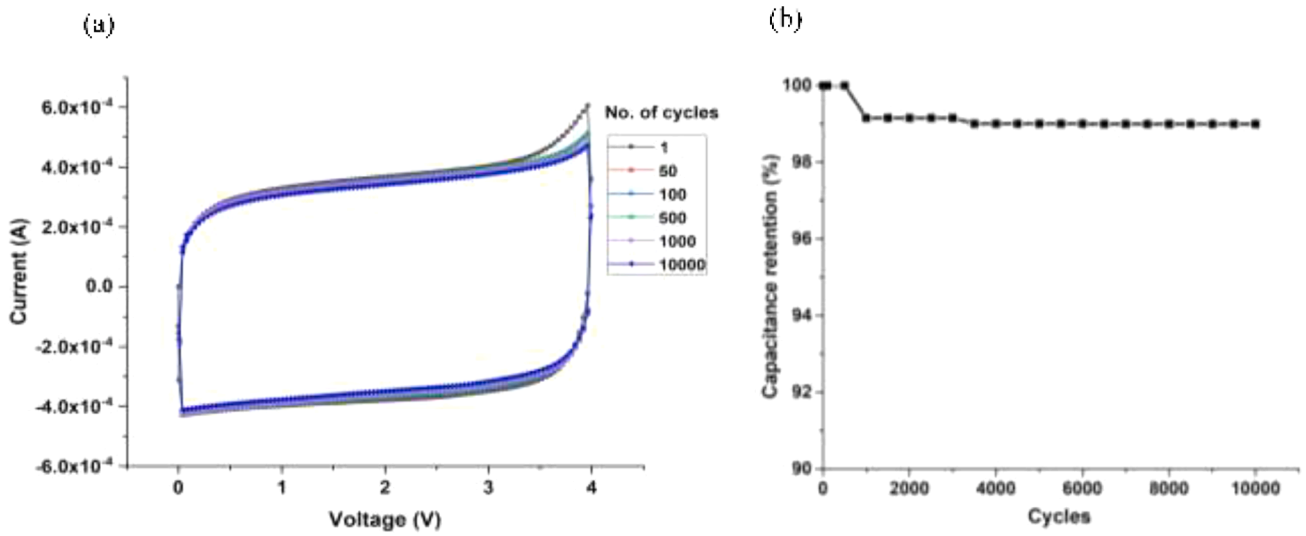

Fig. 6. Cyclic voltammetry graphs from 1 to 10,000 cycles (a), Change in capacitance as a function of cycle number (b).

For an ideal capacitor, the real part of *Z* is zero, so the Nyquist plot shows a vertical line only coinciding with the vertical axis. In practice, total impedance consists of real and imaginary values described in Eq. (3) where the impedance's real part is referred to as equivalent series resistance (ESR).

$$Z = \sqrt{Z'^2 + Z''^2} \tag{3}$$

Where, Z' is the real part and Z'' is the imaginary part of the impedance.

The almost vertical line observed at low frequency is characteristic for ideal capacitance. A slope line of 45° was observed at the intermediate frequency due to the porous structure of active material and is characteristic of the distributed resistance. This region is also called the Warburg diffusion region. The steeper the slope is, the higher is the diffusion capability of ions entering the pores [40]. A semi-circle loop was observed at high frequencies, from 1 kHz to 1 MHz. The shape of the loop is similar in all four DCSCs, and the center of the semicircle lies below the real axis; this is caused by the electron transfer limited process. The ESR decreases towards higher frequencies and intersects the real axis Z' shown in Fig. 3(a) Fig. 3.(b) shows a magnified view of the Nyquist plot. The plot of the real and imaginary value of impedance as a function of frequency is shown in Fig. 3(c). The ESR measured for DCSCs was between 1.8 and 2.5 Ω. The components defining the ESR of these DCSCs were distributed resistance in the porous active material, contact resistance between the active material and current collector, and the resistance of current collector and electrolyte [8,21,41,42]. The components contributing to the total ESR of the DCSCs can be studied with the Randels circuit model. The Randles circuit model is commonly used in EIS for interpretation of impedance spectra.The circuit model as shown in Fig. 4(a) and Nyquist plot of fitted and measured values for imaginary and real impedance are shown in Fig. 4(b). The circuit model helps in the analysis of bulk resistance (current collector and solution resistance) denoted as R_s and charge transfer resistance denoted as R_c, and Warburg diffusion region resistance denoted as W. In this model, the series element R_c and W are connected with capacitor C in parallel. This parallel combination is connected in series with R_s shown in Fig. 4 (a) [42].

The value of bulk resistance (current collector and electrolyte) R_s was from 0.5 to 1 Ω (left most intersect of real axis),) and the charge transfer resistance, R_c was from 1.2 to 1.4 Ω (width of semicircle). Finally, the value of distributed resistance in the Warburg diffusion region (W) was measured to be from 0.2 to 0.4 Ω at the 45° line segment.

A Bode plot of the DCSCs related to the impedance and phase behavior over a frequency range from 1 Hz to 100 kHz is given in Fig. 5. The impedance was high at the low frequency region and decreased with increasing frequency because the impedance of the supercapacitors is inversely proportional to the frequency. At the highest frequency, the ohmic resistance dominates the impedance and the impedance value is constant [34]. The impedance-frequency plot was similar in all four DCSC devices. The phase angle value for devices was from 79.5 ° to 81 °. This value is close to the ideal capacitor value of -90 °. Thus, it indicates the nearly capacitive nature of the device. At a phase angle of -45 °, the resistance and reactance of the devices have equal magnitude. Hence, from the phase-frequency plot diagram, the characteristic frequency at an angle of -45 ° is about 22 Hz to 32 Hz. This corresponds to the relaxation time denoted as t_o about 31 to 45 ms ($t_o = f_o^{-1}$). The relaxation time is the minimum time needed to discharge the energy from the capacitor with an efficiency over 50 % of its maximum value [43].

3.3. Leakage current

To measure leakage current in our DCSCs, 5 V voltage was applied over them for 24 h and the small float current required to maintain that voltage level was recorded as leakage current. The leakage current was determined using the industrial standard IEC 62391-1 [44]. The measured electrical parameters of DCSCs devices are shown in Table 1. The measured leakage current was very low, between 0.1 μA and 0.3 μA. One possible cause of the small residual leakage current is from impurities that undergo Faradiac charge-transfer reactions at the electrodes. The impurities may be transition metal ions, which are commonly found in carbon materials [4]. The devices were assembled in inert atmosphere (glove box) to avoid oxygen and water contamination that would be possible in ambient air. Robust sealing of the DCSCs is essential and prevents impurities from entering the devices. This was achieved through hot melt sealing during device assembly.

3.4. Life-time test

In order to measure the cyclic stability of the DCSC, we performed cyclic voltammetry from 1 to 10,000 cycles at a scan rate of 100 mV/s. We observed a relatively symmetric rectangular cyclic sweep, as shown in Fig. 6(a), which is indicative of good capacitor behavior. The percentage of change in capacitance as the function of cyclic count is shown in Fig. 6(b); as can be seen, the capacitance value decreases only by 1% from the original value after 10,000 cycles, thus the capacitance of the DCSC reported here is quite stable under cycling.

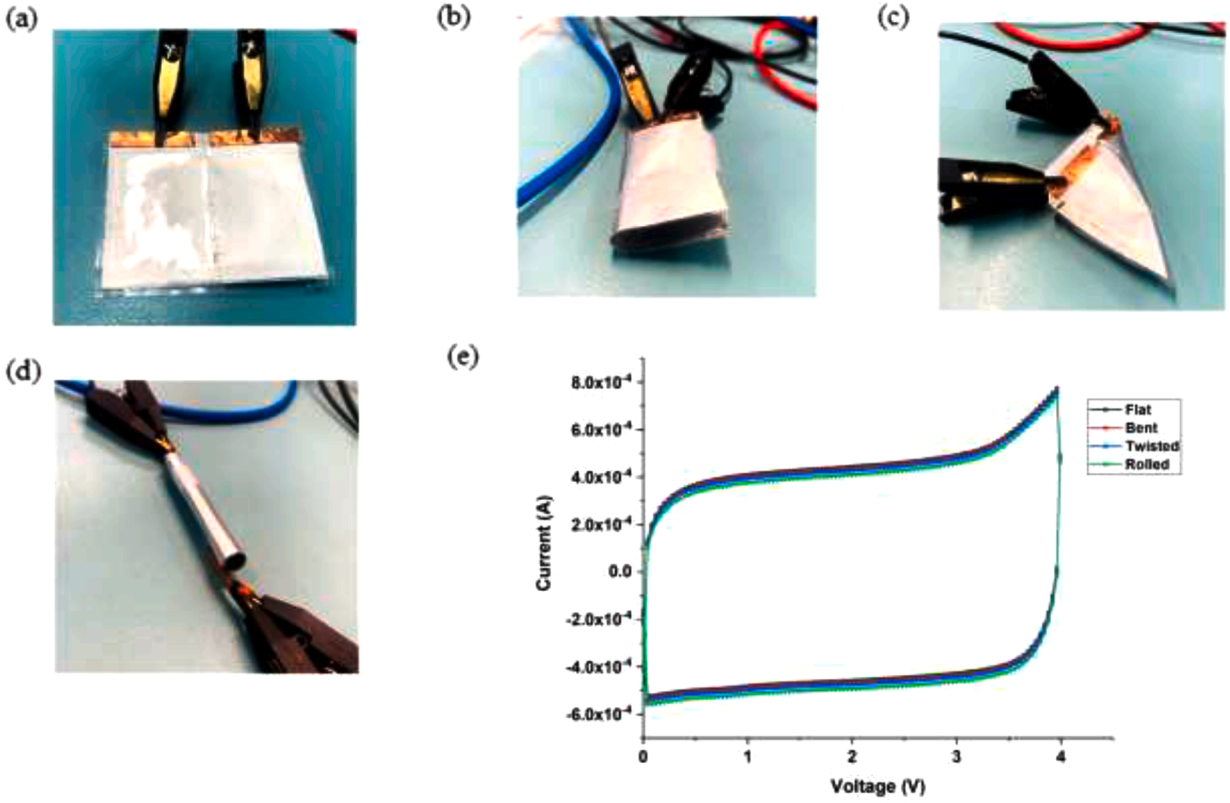

Fig. 7. DCSC under different mechanical deformations: Flat (a), Bent (b), Twisted (c), Rolled (d) and CV measurements graphs of deformed DCSC (e).

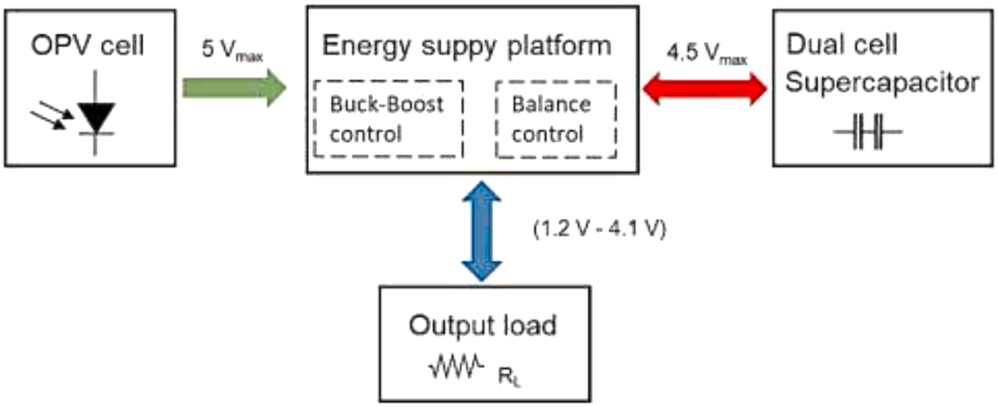

Fig. 8. Schematic view of energy supply platform system with harvester, dual cell supercapacitor and output load unit.

3.5. Mechanical and electrical reliability

Flexibility is a significant property for a printed supercapacitor in many practical applications of electronics. To evaluate the potential and the flexibility of the DCSC for flexible energy storage under real conditions, a mechanical deformation test was performed. The DCSC was bent, twisted and rolled with small curvature radius of 0.5 cm as shown in Fig.7. Cyclic voltammetry was measured at 100 mV/s (0–4 V) to observe the electrical behavior of the DCSC during these mechanical deformations. The cyclic voltammetry curves are almost identical to those measured for unbent devices, indicated excellent mechanical and electrical stability under bending.

3.6. Integration of energy harvester with dual cell supercapacitor

A schematic representation of the energy harvester (OPV module), integrated energy supply platform and dual cell supercapacitor is shown in Fig. 8.

Table 2
MPPT ratio based on the characteristic of the input source.

Config. 1	Config. 2	MPPT
0	0	70%
0	1	75%
1	0	85%
1	1	90%

The ESP comprises an AEM10941 harvesting IC, which is suitable for indoor applications because it has ultra-low power startup. The accepted working voltage range of the ESP is between 0.3 V and 5 V. The OPV cell acts as an energy source. The ESP acts as an interface between OPV and the DCSC storage unit. The ESP uses a maximum power point tracking

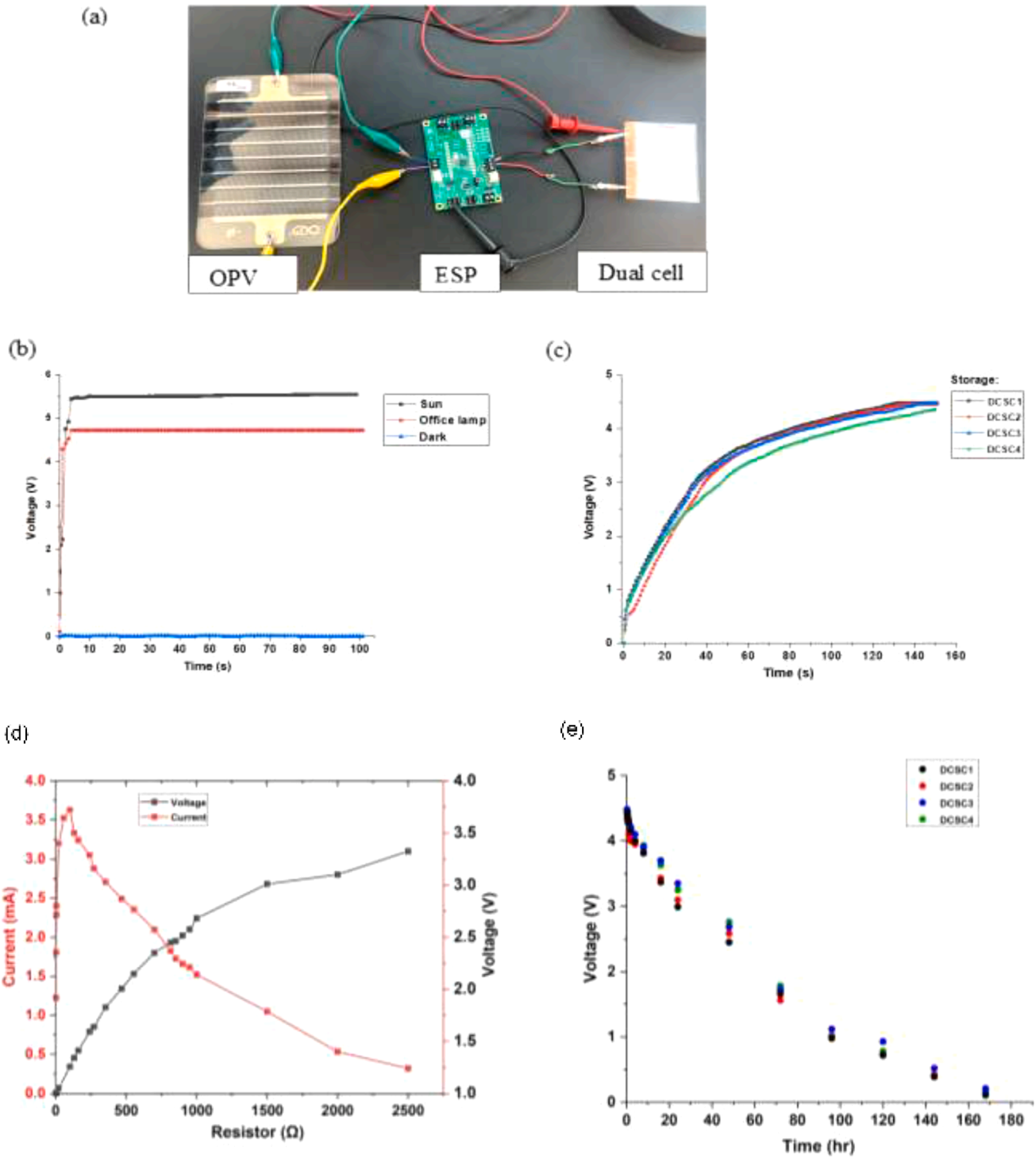

Fig. 9. Photograph of integration of OPV, ESP and dual cell supercapacitor (a), Open circuit voltage measurement of OPV cell under the sun, office lamp and in dark (b), Voltage measured across four dual cell supercapacitors (DCSC) as a function of time (c), Relationship between the output current-voltage and resistor (d), Self-discharge measurement of DCSCs (e).

(MPPT) algorithm to get the most power out of the solar cells. Based on the characteristic of the input power source, the MPPT configuration can be selected as shown in Table 2. The boost converters raise the voltage to a level suitable for charging the DCSC in the range between 2.2 V and 4.5 V. The low drive out (LDO) is available to power loads at different operating voltages between 1.2 V and 4.1 V at a maximum current of 20 mA to 80 mA. When the DCSC voltage reaches the maximum value of 4.5 V, the charge is completed, and internal logic prevents damage to the storage element and to the internal circuitry. If the DCSC is discharged below 2.2 V, the LDO is power gated to shut down mode and protects the storage element from further discharge [23].

A photograph of the circuit connection of OPV cell, ESP and DCSC is shown in Fig. 9(a). Initially, the open-circuit voltage of the OPV cell was measured at three different conditions: direct sun, office lamp and in dark. The measured output voltage under direct sun and office lamp is about 5.5 V and 4.8 V, respectively, as shown in Fig. 9(b). The plot of output current and voltage of the OPV across the external load resistance in the range 1–2.5 kΩ is shown in Fig. 9(d). The maximum output

Table 3
Calculation of voltage measured and energy harvested across the four DCSCs.

S/N	Capacitance (mF)	Voltage (V_{DCSC})	V_{DCSC} (%)	Energy harvested (mJ)
DCSC1	3.0	4.49	99.7	30.2
DCSC2	3.6	4.45	98.8	35.6
DCSC3	3.9	4.47	99.3	39.0
DCSC4	4.0	4.35	96.6	37.8

current of 3.72 mA was obtained at a resistance about 100 Ω. Similarly, the maximum power was 5.2 mW at load resistor 1 kΩ. As we are focusing on indoor light energy harvesting, the voltage range is enough to power the ESP unit. The OPV was irradiated with a 7.7 W LED lamp having luminous flux of 806 lm, positioned at a distance of about 30 cm. The voltage across the DCSCs as a function of time is shown in Fig. 9(c). The measured maximum voltage of DCSCs was from 4.35 V to 4.49 V and the logic circuit prevents DCSC from further charging by disabling the boost converter and maintaining charge balance. The energy harvested in the DCSC is given by Eq. (4).

$$E = \frac{1}{2}CV^2 \tag{4}$$

where C is the capacitance and V is the voltage measured across the DCSC

The measured voltage and energy harvested are shown in Table 3. The self-discharge behavior of the supercapacitor was measured over a period of one week. The self-discharge behavior was similar in all supercapacitors. The plot of voltage over time is shown in Fig. 9(e). The maximum charge voltage was 4.5 V, which decreases to below 1 V after 4 days. This is a more rapid decay of voltage than has been seen in larger supercapacitors and is due to the small capacitance (3 to 4 mF). Self-discharge phenomena such as Ohmic leakage (shunt resistance), or diffusion-controlled self-discharge due to the presence of impurities in carbon, make a relatively larger contribution to self-discharge in low-capacitance devices. Ricketts et al. reported quite rapid self-discharge in an organic electrolyte-based supercapacitor and mentioned that the diffusion process causes a significant loss of stored energy [45]. Details about the self-discharge mechanism in supercapacitors have been reported earlier [4,45,46].

Fig. 10(a) shows a photograph of a practical demonstration of an energy harvester unit operating a low power device. In this experiment, a LED was connected to the ESP unit. Once the DCSC reaches a voltage of about 3.6 V, the LDO is turned on and provides peak power to the LED. The LED blinks for a few seconds and the voltage measured across the led was 2.5 V. The voltage of the LED as a function of time is shown in Fig. 10(b). The peak power generated by the circuit was about 20 mW. This demonstrates that the energy module delivers sufficient energy, even under indoor lighting conditions, to operate low-power portable devices.

4. Conclusion

In this work, we designed an organic electrolyte-based, printable, and flexible dual cell supercapacitor (DCSC), to fulfill the requirements of higher voltage, low ESR and low leakage current. The DCSC is environmentally friendly, manufactured by low-cost printing and coating methods, and fabricated at relatively low temperature (<100 °C). In addition, we have demonstrated an energy harvesting system through the integration of flexible OPV, printed dual cell supercapacitor and energy supply platform. The ESP is capable of tracking maximum power from OPV (MPPT), DC-DC boost of OPV output, charge our supercapacitor efficiently and operate the load device through a low drive output (LDO) unit. The printed 3 to 4 mF DCSC is sufficient to store energy and power a LED. The maximum energy harvested from the harvester was about 39 mJ. This energy is enough for powering portable electronic devices and sensors. DCSCs are mechanically stable, and the devices are well suited for flexible energy storage. In cycle life test up to 10,000 cycles, DCSCs show good performance with about 99 % capacitance retention.

Author statement

All authors have participated in (a) conception and design, or analysis and interpretation of the data; (b) drafting the article or revising it critically for important intellectual content; and (c) approval of the final version. Furthermore, each author certifies that this material has not been and will not be submitted to or published in any other publication.

Declaration of Competing Interest

All authors have participated in (a) conception and design, or analysis and interpretation of the data; (b) drafting the article or revising it critically for important intellectual content; and (c) approval of the final version. This manuscript has not been submitted to, nor is under review at, another journal or other publishing venue. The authors have no affiliations with or involvement in any organization or entity with any financial interest (such as honoraria; educational grants; participation in speakers' bureaus; membership, employment, consultancies, stock ownership, or other equity interest; and expert testimony or patent-licensing arrangements), or non-financial interest (such as personal or

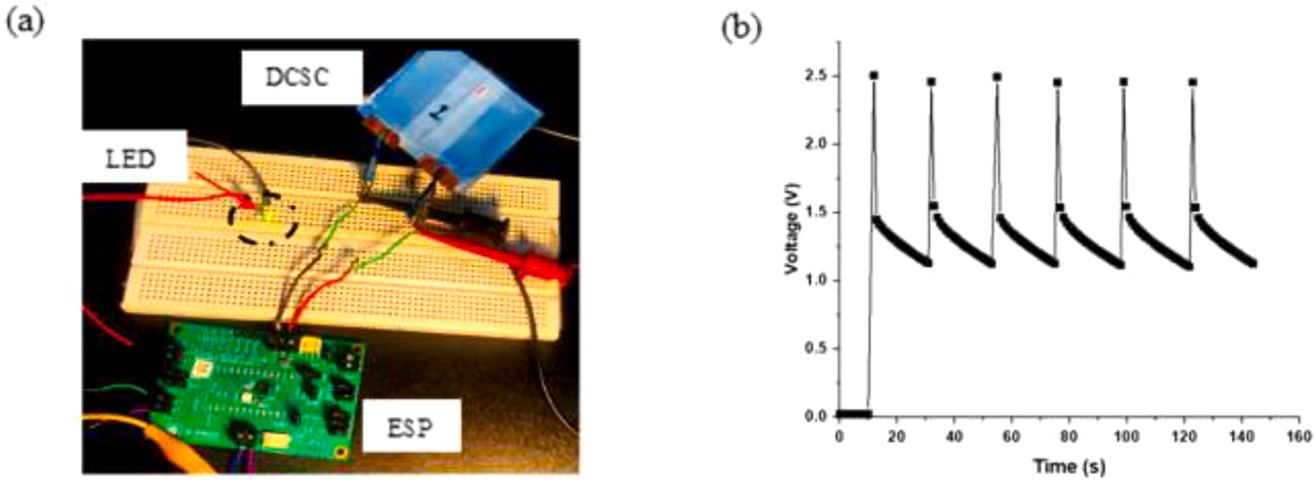

Fig. 10. Photograph of energy harvester unit powering a LED (a), Peak voltage measured across LED as a function of time (b).

professional relationships, affiliations, knowledge or beliefs) in the subject matter or materials discussed in this manuscript.

Acknowledgment

This work was financially supported from the European Union's Horizon 2020 research and innovation programme under grand agreement n 825143, project Smart2Go. We also thank to Mr. Markus Tuomikoski (VTT) and Mr. Andreas Tschepp (Joanneum Research) for helpful discussions related to energy harvesting and integration.

References

[1] M. Aneke, M. Wang, Energy storage technologies and real life applications – a state of the art review, Appl. Energy 179 (2016) 350–377, https://doi.org/10.1016/j.apenergy.2016.06.097.
[2] K. Hung, C. Masarapu, T. Ko, B. Wei, Wide-temperature range operation supercapacitors from nanostructured activated carbon fabric, J. Power Sources 193 (2) (2009) 944–949, https://doi.org/10.1016/j.jpowsour.2009.01.083.
[3] S. Wang, T. Wei, Z. Qi, Supercapacitor energy storage technology and its application in renewable energy power generation system, in: Proceedings of the ISES World Congress 2007, 2009, pp. 2805–2809, https://doi.org/10.1007/978-3-540-75997-3_566. I – VolV.
[4] J. Keskinen, et al., Architectural modifications for flexible supercapacitor performance optimization, Electron. Mater. Lett. 12 (6) (2016) 795–803, https://doi.org/10.1007/s13391-016-6141-y.
[5] K. Krishnamoorthy, P. Pazhamalai, V. K. Mariappan, S. Manoharan, D. Kesavan, and S. Kim, "Two-dimensional Siloxene – rraphene heterostructure-based high-performance supercapacitor for capturing regenerative braking energy in electric vehicles," doi: 10.1002/adfm.202008422.
[6] H. Moon, et al., Ag/Au/polypyrrole core-shell nanowire network for transparent, stretchable and flexible supercapacitor in wearable energy devices, Sci. Rep. 7 (1) (2017) 41981, https://doi.org/10.1038/srep41981.
[7] J. Keskinen, et al., Asymmetric and symmetric supercapacitors based on polypyrrole and activated carbon electrodes, Synth. Met. 203 (2015) 192–199, https://doi.org/10.1016/J.SYNTHMET.2015.02.034. May.
[8] R. Kötz, M. Hahn, R. Gallay, Temperature behavior and impedance fundamentals of supercapacitors, J. Power Sources 154 (2) (2006) 550–555, https://doi.org/10.1016/j.jpowsour.2005.10.048.
[9] X.H. Li, Y.Z. Meng, Q. Zhu, S.C. Tjong, Thermal decomposition characteristics of poly(propylene carbonate) using TG/IR and Py-GC/MS techniques, Polym. Degrad. Stab. 81 (1) (2003) 157–165, https://doi.org/10.1016/S0141-3910(03)00085-5.
[10] H.V.T. Nguyen, J. Kim, K.K. Lee, High-voltage and intrinsically safe supercapacitors based on a trimethyl phosphate electrolyte, J. Mater. Chem. A (2021) 20725–20736, https://doi.org/10.1039/d1ta05584d.
[11] C. Shi, et al., An 'all-in-one' mesh-typed integrated energy unit for both photoelectric conversion and energy storage in uniform electrochemical system, Nano Energy 13 (2015) 670–678, https://doi.org/10.1016/j.nanoen.2015.03.032.
[12] A. Nechibvute, A. Chawanda, P. Luhanga, Piezoelectric energy harvesting devices: an alternative energy source for wireless sensors, Smart Mater. Res. 2012 (2012) 1–13, https://doi.org/10.1155/2012/853481.
[13] C. Rokaya, P. Schaeffner, S. Tuukkanen, J. Keskinen, and D. Lupo, "Motion energy harvesting and storage system including printed piezoelectric film and supercapacitor," 2019, doi: 10.1109/IFETC46817.2019.9073717.
[14] M. Arvani, et al., Flexible energy supply for distributed electronics powered by organic solar cell and printed supercapacitor, in: Proceedings of the IEEE Conference on Nanotechnology, 2020, https://doi.org/10.1109/NANO47656.2020.9183493, 2020-July.
[15] T.D. Nielsen, C. Cruickshank, S. Foged, J. Thorsen, F.C. Krebs, Business, market and intellectual property analysis of polymer solar cells, Sol. Energy Mater. Sol. Cells 94 (10) (2010) 1553–1571, https://doi.org/10.1016/j.solmat.2010.04.074.
[16] Y. Yang, et al., Self-charging flexible solar capacitors based on integrated perovskite solar cells and quasi-solid-state supercapacitors fabricated at low temperature, J. Power Sources 479 (September) (2020), 229046, https://doi.org/10.1016/j.jpowsour.2020.229046.
[17] Z. Tian et al., "Printable magnesium ion quasi-solid-state asymmetric supercapacitors for flexible solar-charging integrated units," no. 2019, pp. 1–11, doi: 10.1038/s41467-019-12900-4.
[18] B. Pozo, I. Garate, Á. Araujo, and S. Ferreiro, "Energy harvesting technologies and equivalent electronic structural models — review," 2019.
[19] R.M. Ferdous, A.W. Reza, M.F. Siddiqui, Renewable energy harvesting for wireless sensors using passive RFID tag technology: a review, Renew. Sustain. Energy Rev. 58 (2016) 1114–1128, https://doi.org/10.1016/j.rser.2015.12.332.
[20] InfinityPV, "organic solar cell." https://infinitypv.com/11-products/infinitypro/index.php.
[21] T. Chen et al., "An integrated energy wire for both photoelectric conversion and energy storage," vol. 51, pp. 11977–11980, 2012, doi: 10.1002/anie.201207023.
[22] J. O. Thostenson et al., "Integrated flexible conversion circuit between a flexible photovoltaic and supercapacitors for powering wearable sensors integrated flexible conversion circuit between a flexible photovoltaic and supercapacitors for powering wearable sensors," 2018, doi: 10.1149/2.0141808jes.
[23] Epeas, "Solar energy harvesting." https://e-peas.com/product/aem10941/.
[24] J. Keskinen, et al., Printed supercapacitors on paperboard substrate, Electrochim. Acta 85 (2012) 302–306, https://doi.org/10.1016/j.electacta.2012.08.076.
[25] S. Lehtimäki, A. Railanmaa, J. Keskinen, M. Kujala, S. Tuukkanen, D. Lupo, Performance, stability and operation voltage optimization of screen-printed aqueous supercapacitors, Sci. Rep. 7 (2017), https://doi.org/10.1038/srep46001.
[26] M. Arvani, J. Keskinen, A. Railanmaa, S. Siljander, T. Björkqvist, S. Tuukkanen, Additive manufacturing of monolithic supercapacitors with biopolymer separator, J. Appl. Electrochem. (2020), https://doi.org/10.1007/s10800-020-01423-2, 0123456789.
[27] Y. Tian, X. Li, Y. Zhu, R. Xia, Optimal capacity allocation of multiple energy storage considering microgrid cost, J. Phys. Conf. Ser. 1074 (1) (2018), https://doi.org/10.1088/1742-6596/1074/1/012126.
[28] A. Railanmaa, et al., Skin-conformable printed supercapacitors and their performance in wear, Sci. Rep. 10 (1) (2020) 1–9, https://doi.org/10.1038/s41598-020-72244-8.
[29] X. Sun, X. Zhang, H. Zhang, B. Huang, Y. Ma, Application of a novel binder for activated carbon-based electrical double layer capacitors with nonaqueous electrolytes, J. Solid State Electrochem. 17 (7) (2013) 2035–2042, https://doi.org/10.1007/s10008-013-2051-1.
[30] C. Rokaya, J. Keskinen, C. Bromels, P. Sch ffner, E. Küzeci, D. Lupo, Polymer-based printed electrolytic capacitor and its circuitry application in a low pass filtering, rectifying and energy storage unit, Flex. Print. Electron. 6 (2) (2021) 25005, https://doi.org/10.1088/2058-8585/ac023d.
[31] W. Wang, et al., Hierarchical core–shell Co_3O_4/graphene hybrid fibers: potential electrodes for supercapacitors, J. Mater. Sci. 53 (8) (2018) 6116–6123, https://doi.org/10.1007/s10853-017-1971-z.
[32] Y. Liu, et al., High-performance flexible all-solid-state supercapacitor from large free-standing graphene-PEDOT/PSS Films, Sci. Rep. 5 (1) (2015) 17045, https://doi.org/10.1038/srep17045.
[33] X. Hu, Y. Chen, Z. Hu, Y. Li, and Z. Ling, "All-solid-state supercapacitors based on a carbon-filled porous/dense/porous layered ceramic electrolyte," vol. 165, pp. 1269–1274, 2018, doi: 10.1149/2.0481807jes.
[34] K.P. Radha, Magnitude Bode Plot analysis of solid polymer electrolyte PMMA complexed with adipic acid, Der Pharma Chem. (2016) 4–9. January.
[35] N.K. Sidhu, A.C. Rastogi, Bifacial carbon nanofoam-fibrous PEDOT composite supercapacitor in the 3-electrode configuration for electrical energy storage, Synth. Met. 219 (2016) 1–10, https://doi.org/10.1016/j.synthmet.2016.04.012. May 2018.
[36] B.A. Abdulkadir, J.O. Dennis, M.F.B.A. Shukur, M.M.E. Nasef, F. Usman, Study on dielectric properties of gel polymer electrolyte based on PVA-K2CO3 composites, Int. J. Electrochem. Sci. 16 (1) (2021) 1–15, https://doi.org/10.20964/2021.01.34.
[37] C. H. Chan, "Characterization of polymer electrolytes by dielectric response using electrochemical impedance spectroscopy," no. February, 2018, doi: 10.1515/pac-2017-0911.
[38] P. Kurzweil, H.J. Fischle, A new monitoring method for electrochemical aggregates by impedance spectroscopy, J. Power Sources 127 (1–2) (2004) 331–340, https://doi.org/10.1016/j.jpowsour.2003.09.030.
[39] G. Porzi, C. Concilio, Halogen-metal interconversion in 2,7-dibromonaphthalene and 2,7-dibromoanthracene, J. Organomet. Chem. 128 (1) (1977) 95–98, https://doi.org/10.1016/S0022-328X(00)92039-4.
[40] A. Awitdrus, M. Suleman, N. Syahirah, S. Shamsudin, Energy and power of supercapacitor using carbon electrode deposited with nanoparticles nickel oxide, Int. J. Electrochem. Sci. 11 (1) (2016) 95–110.
[41] S. Lehtimäki, A. Railanmaa, J. Keskinen, M. Kujala, S. Tuukkanen, D. Lupo, Performance, stability and operation voltage optimization of screen-printed aqueous supercapacitors, Sci. Rep. 7 (2017) 1–9, https://doi.org/10.1038/srep46001. Apr.
[42] W. Choi, H.C. Shin, J.M. Kim, J.Y. Choi, W.S. Yoon, Modeling and applications of electrochemical impedance spectroscopy (EIS) for lithium-ion batteries, J. Electrochem. Sci. Technol. 11 (1) (2020) 1–13, https://doi.org/10.33961/jecst.2019.00528.
[43] W. Hua, et al., Micro-supercapacitors based on oriented coordination polymer thin films for AC line-filtering, RSC Adv. 8 (53) (2018) 30624–30628, https://doi.org/10.1039/c8ra06474a.
[44] IEC 62391-1, "International standard : fixed electric double-layers capacitors for use in electronic equipment-Part 1: generic specification," 2006.
[45] B.W. Ricketts, C. Ton-That, Self-discharge of carbon-based supercapacitors with organic electrolytes, J. Power Sources 89 (1) (2000) 64–69, https://doi.org/10.1016/S0378-7753(00)00387-6.
[46] M. Haque, et al., Identification of self-discharge mechanisms of ionic liquid electrolyte based supercapacitor under high-temperature operation, J. Power Sources 485 (2020) 2021, https://doi.org/10.1016/j.jpowsour.2020.229328. December.